Hindawi
International Journal of Aerospace Engineering
Volume 2021, Article ID 6685635, 15 pages
https://doi.org/10.1155/2021/6685635

Research Article

Kinematic Singularity and Bifurcation Analysis of Sidestay Landing Gear Locking Mechanisms

Kui Xu, Yin Yin, Yixin Yang, Hong Nie, and Xiaohui Wei

State Key Laboratory of Mechanics and Control of Mechanical Structures, Key Laboratory of Fundamental Science for National Defense-Advanced Design Technology of Flight Vehicle, Nanjing University of Aeronautics and Astronautics, Nanjing 210016, China

Correspondence should be addressed to Hong Nie; hnie@nuaa.edu.cn

Received 19 November 2020; Revised 16 March 2021; Accepted 17 June 2021; Published 4 August 2021

Academic Editor: Jun-Wei Li

A dual-sidestay landing gear is prone to locking failure in the deployed state due to the restriction of movement between two sidestays. However, the principle of its locking movement still remains unclear. The present study is aimed at investigating the synchronous locking performance of the dual-sidestay landing gear based on the singularity and bifurcation theory. From the perspective of the kinematic mechanism, the reason for high sensitivity to structural dimensions in the locking process is explained, and the locked position is investigated by employing the numerical continuation method in the case of a single-sidestay landing gear. Afterwards, the reason for the locking failure of the dual-sidestay landing gear is analyzed, and a kinematic optimization method for the synchronous locking is proposed. The results reveal that the lock links must reach the lower overcenter singular point to fully lock the landing gear, and the singular point is sensitively affected by structural parameters. Owing to the different positions of singular points, the movements of fore and aft sidestays seriously restrict each other, causing locking failure of the dual-sidestay landing gear. The singular points of two sidestays can be optimized to be approximately identical, making their movements more coordinated.

1. Introduction

A supercritical wing is extensively used in large aircraft for attaining better aerodynamic performance [1, 2]. For the supercritical wing, however, the stowage for the landing gear is considerably smaller than that for the conventional wing. Narrow space signifies that a conventional planar (2D) landing gear can hardly comply with the design requirements, since the sidestay links are located above the main strut after folding, which occupy a large vertical space, as shown in Figure 1(a). In contrast, for a three-dimensional (3D) landing gear, the sidestay plane can be rotated about a specific axis, so that it is overall folded over the side of the main strut. As a result, the 3D landing gear excellently reduces the size of the vertical space, as shown in Figure 1(b).

The extensive use of composite material has contributed hugely to the reduction in aircraft weight. A composite wing, however, does not carry as much ground load as a metallic one. From the load transfer perspective, the ground impact load should not be borne entirely by the wing. Thus, a dual-sidestay (DS) landing gear is used to transfer ground load to the wing and fuselage [3, 4]. Compared to a single-sidestay (SS) landing gear, the DS landing gear has an additional sidestay, as shown in Figure 2, and the motion coordination between fore and aft sidestays appears particularly important. In the case of an unreasonable design of structural parameters, the two sidestays can hinder and constrain each other, disallowing its complete locking. Hence, it is imperative to investigate the motion coordination between two sidestays.

The multidisciplinary time-domain cosimulation technology [5–7] has often been adopted to research landing gear mechanisms. However, this approach requires substantial iterations in handling highly nonlinear problems, which is time- and labour-consuming. Numerical continuation [8, 9] has been applied to aircraft design for several years [10], which can enable fast and efficient exploration of highly nonlinear problems of the landing gear. Following the initial proposal of this method for analyzing landing gear mechanisms by Knowles et al. [11], the research approach integrating

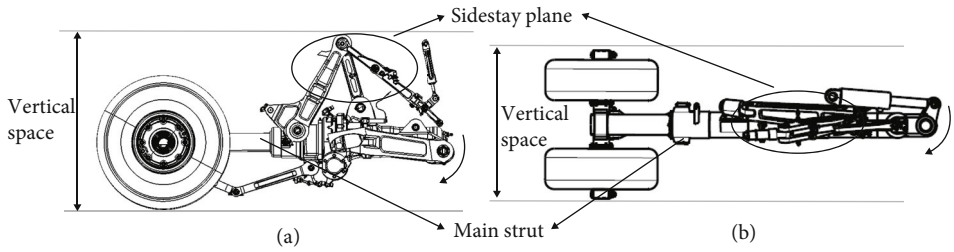

Figure 1: Vertical storage space of 2D versus 3D landing gear.

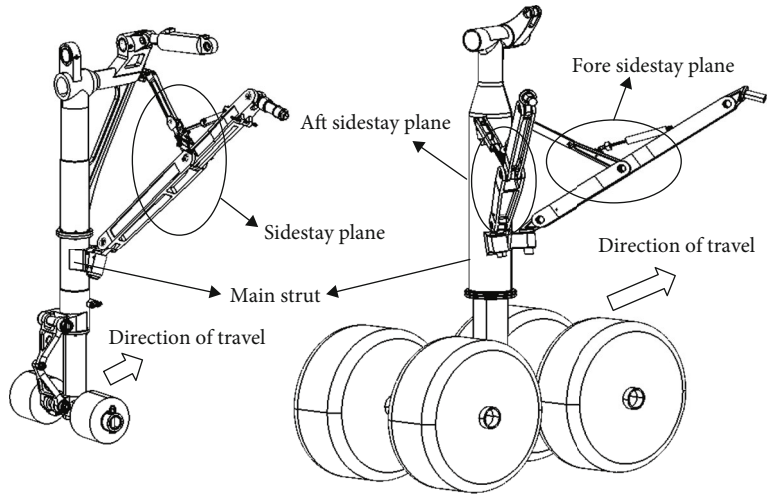

Figure 2: Changes in the DS versus SS landing gears.

numerical continuation and bifurcation analysis has become increasingly mature [12]. Exploiting this method, Knowles et al. [13–16] and Yin et al. [17] analyzed the bifurcation characteristics of different landing gear mechanisms sequentially and concluded that the landing gear would inevitably undergo a jump phenomenon at bifurcation points in the locking process. However, when solving the dynamic equations of the DS landing gear using the numerical continuation method, it has been found that the appearance of bifurcation points does not necessarily imply that two sidestays can be locked synchronously, which indicates the limitation of using the dynamic equations in solving DS mechanisms with extremely high motion sensitivity.

The DS landing gear has several singular points in its retraction cycle, which cause extremely high sensitivity of mechanism motion. Hence, the DS mechanism is analyzed from a kinematic singularity perspective in this paper. Existing methods concerning singularity include the Jacobian matrix method [18], the Grassmann line geometry [19], and the differential geometric theory [20], while attempting to avoid the singular position in the mechanism as far as possible [21, 22]. For instance, Xie et al. [23] and Li and Herve [24] used the above methods to explore the singularity characteristics of different mechanisms. Nevertheless, little literature focuses on the singularity of landing gear mechanisms, particularly the complex spatial DS mechanisms. Therefore, continuation analysis on the kinematics equations of the DS landing gear is performed, and the locked position as well as the underlying jump phenomenon of the mechanism is analyzed from the kinematic singularity and bifurcation perspective in this paper. Furthermore, the fundamental causes of mutual hindrance and restriction between fore and aft sidestays are explained, which can provide crucial guidance for the design of DS landing gear mechanisms.

Initially, the locking performance of a 3D SS mechanism is analyzed. On this basis, the reasons for incomplete locking caused by mutual restriction between two sidestays are investigated. Finally, a novel method for analyzing the synchronous locking of the DS landing gear is developed, which is based on the singularity and bifurcation theory. The structure of this paper is organized as follows: In Section 2, the kinematic model of a 3D SS landing gear mechanism is built, after analyzing its bifurcation and singularity characteristics, and the jump phenomenon and the locked position are analyzed in Section 3. Meanwhile, the effects of structural parameters on the locked position are explored. In Section 4, the principle of mutual hindrance between fore and aft sidestays for the 3D DS landing gear mechanism is investigated based on the foregoing analysis, and the fundamental causes of asynchronous locking are identified. Furthermore, a set of optimal solutions satisfying constraints are given with the aid of multiobjective particle swarm optimization (PSO). The application of the proposed method can effectively achieve the synchronous locking at the initial design phase of DS landing gear mechanisms.

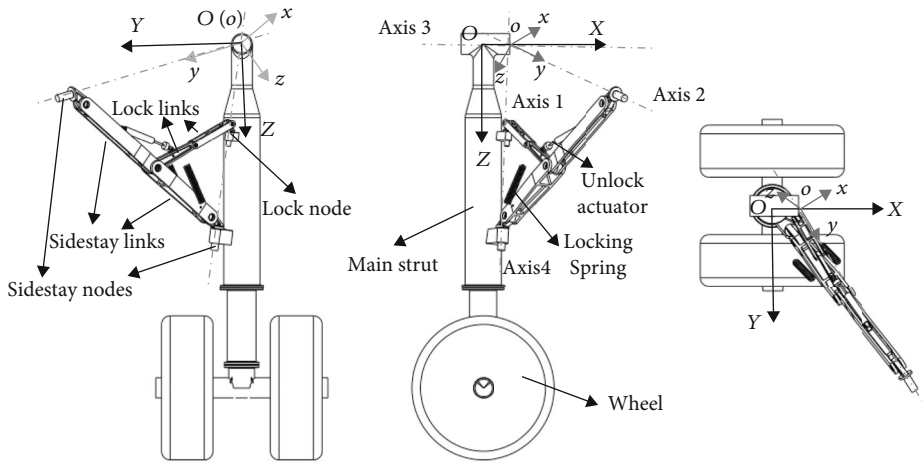

Figure 3: A certain 3D landing gear mechanism.

2. Kinematic Model of the Landing Gear Mechanism

In Figure 3, a certain 3D landing gear mechanism is illustrated, which consists of five links (two sidestay links, two lock links, and a main strut), as well as three nodes (two sidestay nodes and a lock node). These various components are connected via planar revolute joints. To achieve the 3D retraction function, the axes of sidestay nodes (axes 2 and 4 in Figure 3), the axis of the lock node (axis 1), and the rotation axis of the main strut (axis 3) must intersect at one point (point o) [25]. In this way, the motion of sidestay can be always within the same plane. During the retraction cycle of the landing gear, the main strut rotates along the axis 3, while the sidestay not only performs the folding motion but also rotates about the axis 2, so that the rotation plane of the main strut is not in the same plane as the sidestay. The entire retraction and extension processes can be summarized as follows: When retracting the gear, the unlock actuator is needed to unlock the lock links. Then, the retraction actuator can be engaged to allow the main strut to rotate about axis 3, and the sidestay moves accordingly. Finally, the landing gear reaches the deployed position and gets locked. When extending the gear, after upper unlocking, the retraction actuator supplies a pushing force to enable slow extension of the main strut around axis 3. When approaching the lower locked position, the lock links jump from the upper to the lower overcenter state by the action of locking springs, thereby reaching a downlock state. The lock links are equipped with a stop block to prevent excessive downward folding. Eventually, the landing gear stops at the deployed position to complete the locking procedure.

2.1. Coordinate Transformation. Since the rotation plane of the main strut is not in the same plane as the sidestay, it can hardly analyze the mechanism in the same coordinate system. Owing to the fact that the motion of the sidestay is always within the same plane [6, 26], the mechanism model can be divided into different coordinate systems to describe the motion of the main strut and sidestay. The transformation matrix is employed to accomplish the data exchange between them.

Figure 3 presents the establishment of the coordinate systems. In the global coordinate system $O-XYZ$, the origin O is the intersection between the main strut and the axis 3; the X-axis is parallel to axis 3 (positive forward); the Z-axis is aligned with the gravity vector (positive down); and the direction of the Y-axis is determined by the right-hand rule. In the local coordinate system $o-xyz$, the origin o is the intersection point of four axes (axes 1-4); the y-axis is the direction of axis 2; the z-axis is defined to be perpendicular to the y-axis within the sidestay plane; and the direction of the x-axis is determined by the right-hand rule.

With the operation of the landing gear, the main strut rotates about the X-axis, and the sidestay plane rotates about the y-axis. Accordingly, the total transformation matrix T for the global-to-local coordinate system is

$$T = T_0 \cdot T_1, \tag{1}$$

where T_0 is the transformation matrix of the global to the local coordinate system in the initial state (extended, locked position) and T_1 is the transformation matrix of the local coordinate system rotating about the y-axis.

In the initial state, given the presence of both translational and rotational transformations during the global-to-local system conversion, the homogeneous coordinate transformation is adopted herein. Let $\mathbf{e}_1 = [\mathbf{e}_{11}\,\mathbf{e}_{12}\,\mathbf{e}_{13}]^T$ and $\mathbf{e}_2 = [\,\mathbf{e}_{21}\quad \mathbf{e}_{22}\quad \mathbf{e}_{23}\,]^T$ be the base vectors in the global and local systems, respectively, and $\mathbf{o}_\mathbf{O}$ be the vector of origin O in the local system; then,

$$T_0 = \begin{bmatrix} \mathbf{e}_1 \cdot \mathbf{e}_2{}^T & \mathbf{o}_\mathbf{O}{}^T \\ 0 & 1 \end{bmatrix}. \tag{2}$$

Assuming α is the rotation angle of local system about the y-axis, then

$$T_1 = \begin{bmatrix} \cos\alpha & 0 & \sin\alpha & 0 \\ 0 & 1 & 0 & 0 \\ -\sin\alpha & 0 & \cos\alpha & 0 \\ 0 & 0 & 0 & 1 \end{bmatrix}. \quad (3)$$

2.2. Motion Constraint Equations. In Figure 4, the schematic of the landing gear mechanism is presented. The constraint relations between various links can be derived from eight variables $(X_i, Y_i, Z_i, \Theta_i, x_i, y_i, z_i, \text{and } \theta_i)$, where (X_i, Y_i, Z_i) and $(x_i, y_i, z_i)$are the global and local coordinates of the gravity center of the i-th link, respectively; Θ_i denotes the angle between the i-th link and the Z-axis (specifically, Θ_1 is the retraction angle of the main strut); and θ_i is the angle between the i-th link and the y-axis.

Since the global and local coordinates can be interconverted through the coordinate transformation, the position of various links can be identified independently with $(X_i, Y_i, Z_i, \Theta_i)$ or $(x_i, y_i, z_i, \theta_i)$. There are twenty independent geometric variables for the SS mechanism. As the analysis reveals, the mechanism has nineteen independent constraint equations (see Equation (4) and Table 3 in the Appendix), so the degree of freedom (DOF) is one.

$$\begin{bmatrix} X_1 \\ Y_1\text{-}0.5l_1 \cdot \cos\Theta_1 \\ Z_1\text{-}0.5l_1 \cdot \sin\Theta_1 \\ x_2 \\ y_2 - 0.5l_2 \cdot \cos\theta_2 - y_A \\ z_2 - 0.5l_2 \cdot \sin\theta_2 - z_A \\ x_3 \\ y_3 - 0.5l_3 \cdot \cos\theta_3\text{-}y_2 - 0.5l_2 \cdot \cos\theta_2 \\ z_3 - 0.5l_3 \cdot \sin\theta_3\text{-}z_2 - 0.5l_2 \cdot \sin\theta_2 \\ x_4 \\ y_4 + 0.5l_4 \cdot \cos\theta_4\text{-}y_2 - 0.5l_2 \cdot \cos\theta_2 \\ z_4 - 0.5l_4 \cdot \sin\theta_4\text{-}z_2 - 0.5l_2 \cdot \sin\theta_2 \\ x_5 \\ y_5 + 0.5l_5 \cdot \cos\theta_5\text{-}y_4 + 0.5l_4 \cdot \cos\theta_4 \\ z_5 - 0.5l_5 \cdot \sin\theta_5\text{-}z_4 + 0.5l_4 \cdot \sin\theta_4 \\ y_5\text{-}0.5l_5 \cdot \cos\theta_5\text{-}y_E \\ z_5 - 0.5l_5 \cdot \sin\theta_5\text{-}z_E \\ y_3 + 0.5l_3 \cdot \cos\theta_3\text{-}y_C \\ z_3 + 0.5l_3 \cdot \sin\theta_3\text{-}z_C \end{bmatrix} = 0, \quad (4)$$

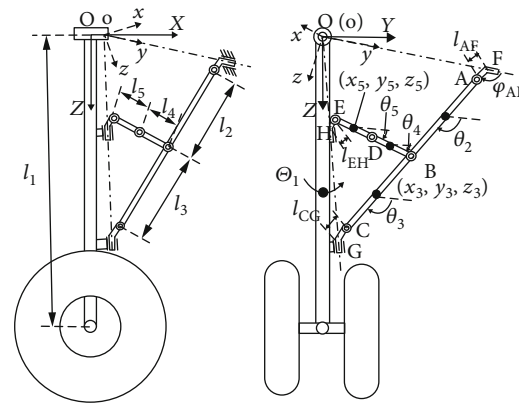

Figure 4: Schematic diagram of the 3D landing gear mechanism.

where l_i denotes the length of the i-th link; y_*, z_* denote the local coordinates of the points $*$ (points A/C/E in Figure 4), which can be derived from the node parameters as follows:

$$\begin{bmatrix} y_A \\ z_A \\ y_C \\ z_C \\ y_E \\ z_E \end{bmatrix} = \begin{bmatrix} y_F + l_{AF} \cdot \cos\varphi_{AF} \\ l_{AF} \cdot \sin\varphi_{AF} \\ y_G\text{-}l_{CG} \cdot \cos\varphi_{CG} \\ z_G\text{-}l_{CG} \cdot \sin\varphi_{CG} \\ y_H\text{-}l_{EH} \cdot \cos\varphi_{EH} \\ z_H\text{-}l_{EH} \cdot \sin\varphi_{EH} \end{bmatrix}, \quad (5)$$

where l_{AF}, l_{CG}, l_{EH} denote the node lengths and $\varphi_{AF}, \varphi_{CG}, \varphi_{EH}$ denote the angles between the node axes and the y-axis. Meanwhile, the local coordinates of points G and H are obtained through coordinate transformation as follows:

$$\begin{bmatrix} x_G \\ y_G \\ z_G \\ 1 \end{bmatrix} = T \cdot \begin{bmatrix} X_G \\ Y_G \\ Z_G \\ 1 \end{bmatrix}, \quad (6)$$

$$\begin{bmatrix} x_H \\ y_H \\ z_H \\ 1 \end{bmatrix} = T \cdot \begin{bmatrix} X_H \\ Y_H \\ Z_H \\ 1 \end{bmatrix}. \quad (7)$$

2.3. Bifurcation Equation of Mechanism Motion. Given the one DOF of the 3D mechanism, Θ_1 is selected as the independent control parameter, while the other variables can be regarded as the state variables. Accordingly, Equation (4) can be rewritten as

$$\mathbf{F}(\mathbf{x}, \lambda) = 0, \quad (8)$$

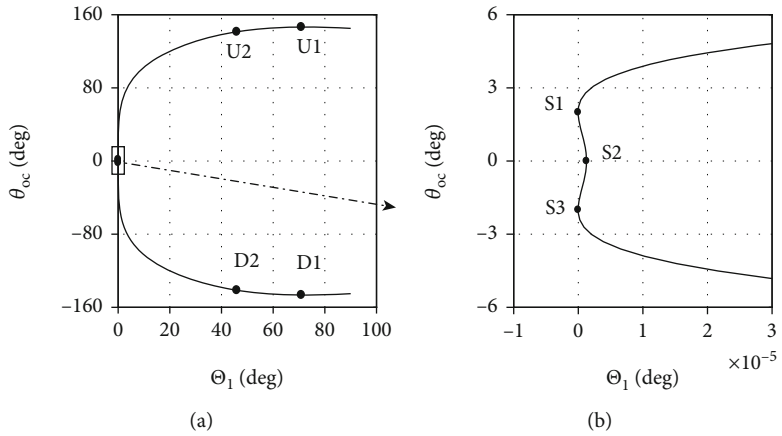

Figure 5: Bifurcation curve of the 3D SS landing gear ((b) presents an enlarged view of the rectangular frame in (a)).

where $\mathbf{x} = (X_1, Y_1, Z_1, x_2, y_2, z_2, \theta_2, \cdots, x_5, y_5, z_5, \theta_5)$ and $\lambda = \Theta_1$.

Equation (8) expresses the variation of state parameter $\mathbf{x}$ with the bifurcation control parameter λ, which is called the bifurcation equation of the 3D mechanism. Utilizing this equation, the bifurcation characteristics of the mechanism can be analyzed.

3. Analysis of the SS Landing Gear Mechanism

3.1. Bifurcation Analysis. The retraction and extension processes of the landing gear can be simulated through numerically continuing Equation (8), and the variation of state parameters (e.g., the overcenter angle $\theta_{oc} = \theta_4$-θ_5 of lock links) with the control parameter Θ_1 can be derived, as shown in Figure 5. For convenience of observation, the kinematic sketches of the mechanism are given in Figure 6, which correspond to various points in Figure 5.

In Figure 5, the motion bifurcation curve is symmetrical about $\theta_{oc} = 0$. The upper half of the curve represents the upward folding of lock links (U1, U2, and S1), while the lower half represents their downward folding (D1, D2, and S3). Three bifurcation points (S1, S2, and S3) appear in the figure, at which two types of motion trends of links are present. As the landing gear extends, it moves along the curve from U1 to U2. At the beginning, Θ_1 changes drastically, while θ_{oc} changes a little. On the contrary, when the landing gear gets close to the deployed state, Θ_1 is almost unchanged, while θ_{oc} changes drastically. Bifurcation occurs when the landing gear moves to the point S1, and two motion branches appear, which correspond to the two motion trends of sidestay links (the dashed lines in Figure 6(c)). The point S1 corresponds to the collinear position of upper and lower sidestay links. At this time, Θ_1 is the smallest, implying that the main strut is extended to the farthest position. By the favorable action of locking springs, the landing gear will move to point S2, at which the upper and lower lock links are collinear. Similarly, two motion branches appear when the mechanism moves to S2, which correspond to the two motion trends of lock links (the dashed lines in Figure 6(d)). When moving to S3 by the action of springs, the upper and lower sidestay links are collinear again, and the lock links are folded down. The appearance of two motion branches of sidestay links is noted (the dashed lines in Figure 6(g)). Generally, the landing gear is provided with a stop block here to prevent further downward motion of lock links, so it is impossible to reach the states D1 and D2 in reality.

3.2. Singularity Analysis. Derivation of Equation (8) with respect to time yields is as follows:

$$\mathbf{A}\,\dot{\mathbf{x}} + \mathbf{B}\,\dot{\lambda} = 0, \tag{9}$$

where $\mathbf{A} = \partial\mathbf{F}/\partial\mathbf{x}$ and $\mathbf{B} = \partial\mathbf{F}/\partial\lambda$. Let $\mathbf{J} = -\mathbf{A}^{-1} \cdot \mathbf{B}$; then,

$$\dot{\mathbf{x}} = \mathbf{J} \cdot \dot{\lambda}. \tag{10}$$

When the mechanism is in a singular position, $\det(\mathbf{A}) = 0$ [27], i.e., $\det(\mathbf{J}) \longrightarrow \infty$. Since the bifurcation points of a mechanism must be in a singular position [28], the points S1, S2, and S3 are the singular positions of the landing gear mechanism. When considering the locking status of lock links, Equation (10) can be rewritten as

$$\dot{\theta}_{oc} = J \cdot \dot{\Theta}_1. \tag{11}$$

It can be seen from Equation (11) that in the vicinity of singular positions, due to $J \longrightarrow \infty$, the lock link speed $\dot{\theta}_{oc}$ is considerably high even if $\dot{\Theta}_1$ is very low. Accordingly, the lock links undergo a quick jump when the landing gear is close to locking. The slope of the curve in Figure 5 can be derived as

$$k = \frac{\partial\theta_{oc}}{\partial\Theta_1} = \frac{\partial\theta_{oc}/\partial t}{\partial\Theta_1/\partial t} = \frac{\dot{\theta}_{oc}}{\dot{\Theta}_1}. \tag{12}$$

The equation of $k = J$ can be derived from Equations (11) and (12). That is, the value of J corresponds to the slope of

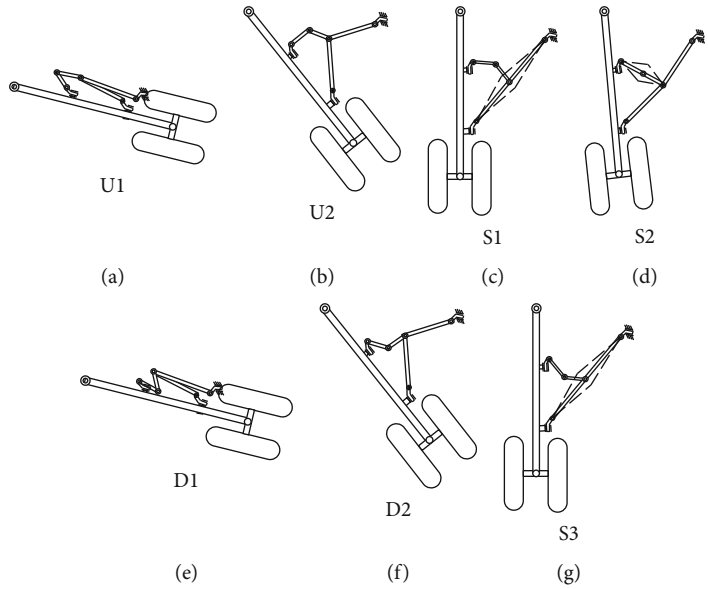

Figure 6: Sketches of the retraction and extension motion of a landing gear: (a) U1; (b) U2; (c) S1; (d) S2; (e) D1; (f) D2; (g) S3.

motion trajectory in Figure 5. Meanwhile, using the principle of virtual work and combining with Equation (11), Equation (13) can be obtained.

$$M_1 = J \cdot M_{\text{oc}}, \tag{13}$$

where M_1 denotes the external moment of the main strut and M_{oc} denotes the internal moment of lock links (centered on the intersection of the lock links).

In the unlocking process of the landing gear, the sidestay links and lock links must be folded. Since the stop block restricts the downward folding of lock links, the lock links can only be folded upwards. Unlocking is impossible to achieve without unlocking the actuator force at the singular points (Figure 7). If the unlocking force is not provided, overcoming the drag load from the upward folding of lock links will be required. This drag load is the equivalent moment M_{oc} of locking springs. From Equation (13), it is clear that $J \cdot M_{oc} \longrightarrow \infty$ when $J \longrightarrow \infty$. In theory, the landing gear can be unlocked only when the external moment M_1 is infinite. In other word, the landing gear will never be unlocked at the singular point. Therefore, the singular feature can be exploited to lock the landing gear near the singular point.

3.3. Analysis of Locked Position. As is clear from the above analysis, the landing gear should be locked near a singular position. A total of three singular positions are present. This section analyzes at which singular position the landing gear should be locked.

The overcenter angle of sidestay links is defined as $\theta_{\text{d}} = \theta_2\text{-}\theta_3$. Figure 8 shows the curves obtained by numerically continuing Equation (8), where θ_{d} is used as the state parameter and Θ_1 is used as the control variable. The black line represents the upward folding of lock links (U1, U2, and S1), whereas the grey line represents the downward folding of lock links (D1, D2, and S3). The black and grey lines overlap each other. Corresponding to Figures 5 and 6, there are three singular points on the motion trajectories. The point S2 is at the intersection of black and grey lines.

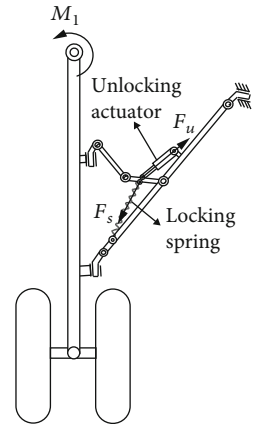

Figure 7: Load analysis at the singular position of landing gear.

The landing gear is highly likely to vibrate during the aircraft take-off, landing, and taxiing [29, 30], so the downlock mechanism must possess a certain function of perturbation resistance. The stop block, as the important component of the downlock mechanism, is mainly used to prevent the excessive motion of lock links. Eventually, the landing gear is locked by the stop block. The locked position can be controlled by setting up the stop block, which is generally arranged at the lock links. To achieve complete locking, the motion of lock links must be restricted in both upward and downward directions. The stop block restricts the downward motion of lock links, while the upward motion is restricted by the structural design and locking springs. In this process, the unlocking of the downlock mechanism can be avoided.

The locked position of landing gear can be analyzed based on Figure 8 combined with Figure 6.

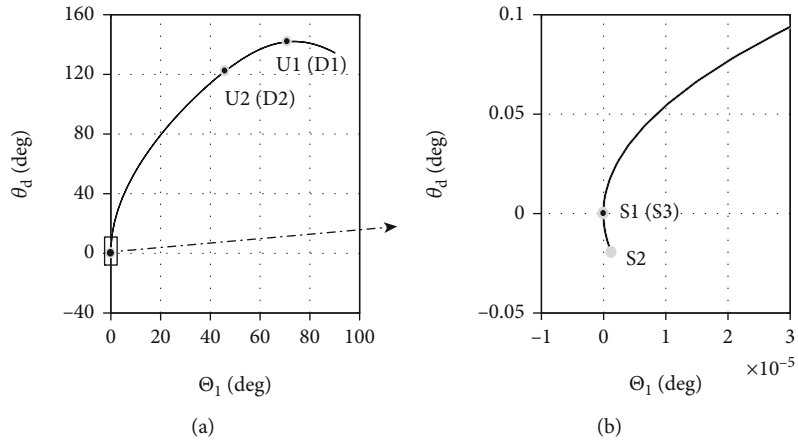

Figure 8: Bifurcation curves for variation of θ_d with Θ_1.

(1) In case the landing gear is locked at the point S1, the stop block will restrict the further downward folding of the lock links and sidestay links. At this time, the upper and lower sidestay links are collinear, while the lock links are in the upper overcenter state. When the sidestay links are subjected to a perturbation to leave the collinear state, they will drive the lock links to fold upward and get unlocked. As is clear from Figure 8, when the sidestay links are subjected to a perturbation of $\Delta\theta_d > 0$, the landing gear will leave the singular point S1, thereby resulting in unlocking

(2) In case the landing gear is locked at the point S2, the stop block will restrict the downward folding of the lock links. At this time, the upper and lower lock links are collinear. It is not difficult to find that when the lock links are subjected to a perturbation to leave the collinear state, they will drive the sidestay links to make $\Delta\theta_d > 0$. Thus, the landing gear will leave the singular point S2, resulting in unlocking. Furthermore, according to the force transmission relationship, the lock links need to bear ground load, which will compromise the reliability of the downlock mechanism [31]

(3) In case the landing gear is locked at the point S3, the stop block will restrict the downward folding of lock links and the upward folding of sidestay links. At this time, the upper and lower sidestay links are collinear again, while the lock links are in the lower overcenter state. When the sidestay links are subjected to a downward perturbation of $\Delta\theta_d < 0$, the lock links will leave point S3 and move to point S2. Although the landing gear will not be unlocked since the lock links will not go beyond point S2, the main strut may rotate due to the perturbation. To diminish the rotation angle, the value of $(\theta_{oc})_{S3}$ should not be excessively large in the deployed state. According to Figure 5, the landing gear is designed to have $(\theta_{oc})_{S3} = 2^\circ$.

To sum up, the locked position of the landing gear should be at the point S3. As described in the foregoing analysis, when the landing gear is at the singular position, the main strut is unable to move regardless of how large the load of the retraction actuator is. If the landing gear is locked at the point S3, it needs to pass the singular points S1 and S2. At this time, the action of locking springs assists in passing the singular points, so that the landing gear does not return along the original trajectory.

3.4. Effects of Structural Parameters on the Locked Position. Once the installation location of the landing gear is decided, the link length parameters will directly affect its locked position (point S3). With changes in the link lengths, the number of singular points also changes accordingly. Thus, selecting appropriate link lengths to ensure the smooth and complete locking of the landing gear is necessary. When considering the effects of link lengths on the point S3, Θ_1 can be treated as a fixed parameter ($\Theta_1 = 0$), where θ_{oc} is used as the state parameter, and the link lengths l_2 and l_4 are used as the control parameters. Figure 9 presents the variation curves of the singular point S3 through numerically continuing Equation (8).

The singular points exhibit a consistent variation trend with the link lengths in the two subfigures. As l_2/l_4 decreases, the points S1 and S3 come together and disappear at the point SN. A new bifurcation point SN appears. As described in the previous section, the landing gear should be locked at the point S3. If the link lengths are decreased past the point SN, the point S3 will disappear, which means failure of locking. Therefore, the feasible range of $l_2 > 549.9$ mm or $l_4 > 249.9$ mm should be selected to accomplish the locking of the landing gear. In addition, it is clear that l_4 is more sensitive to the influence of θ_{oc}.

In actuality, the point SN corresponds to the state of $\theta_{oc} = \theta_d = 0$, as shown in Figure 10(b). The state wherein link lengths are not in the feasible range is shown in Figure 10(a). In this scenario, the landing gear cannot be locked in the deployed position. The point SN is determined jointly by the link lengths. When one of the parameters is changed, the remaining several parameters may also undergo corresponding changes. Their mutual coupling together influences the landing gear locked position. For a more detailed analysis of the effects of link lengths, it can be computed directly by

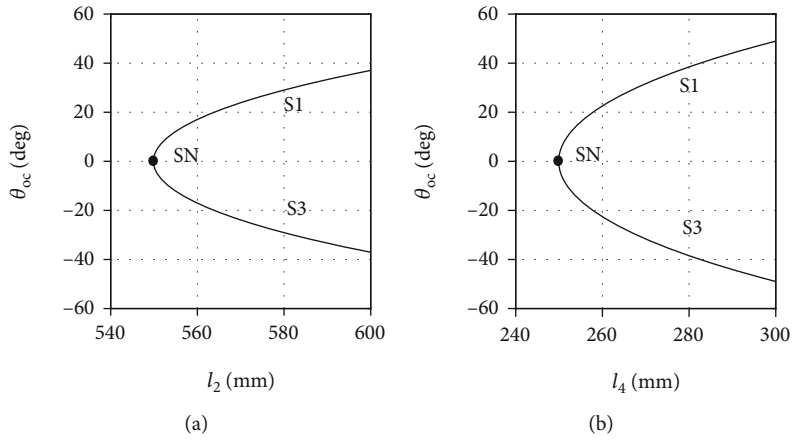

Figure 9: Variations of points S1 and S3 with the link length parameters.

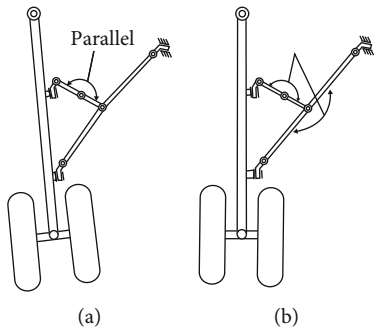

Figure 10: Landing gear mechanism corresponding to the vicinity of point SN.

using two-parameter continuation, thereby obtaining a two-parameter continuation of the point SN locus, as shown by the black line in Figure 11. Figure 11(a) is a 3D view, and Figure 11(b) is the projections of the black curve in the l_2-l_4 plane. With changes in the parameters, the bifurcation point SN changes accordingly, which in turn affects the point S3 as well as the locked position.

From Figure 11(b), it is clear that when the values of l_2 and l_4 locate at the left side of the black curve, points S1 and S3 are absent, implying that the landing gear cannot be locked at the S3 position. In contrast, when the values of l_2 and l_4 locate at the right side of black curve, points S1 and S3 are present, and the landing gear can be fully locked. Consequently, the right side of the curve is the feasible region of link lengths.

The research on the SS landing gear suggests that the lock links must be folded down, in order to achieve full locking. For the SS landing gear, the downward folding motion of lock links will not be hindered due to the promotion by locking springs. In the case of the DS landing gear, however, the sidestay links on both sides may affect each other. Even with the beneficial effect of locking springs, it is highly likely that lock links on the one side undergo locking failure. Hence, the next section carries out research focusing on the DS landing gear.

4. Analysis of DS Landing Gear Mechanism

Compared to the SS landing gear, the DS landing gear will encounter difficulty in synchronous locking of fore and aft sidestays if the additional sidestay is unreasonably designed. An obvious conclusion is that if the fore and aft sidestays are fully symmetrical, their motion trajectories will completely overlap. However, since the ground load needs to be transferred separately to the fuselage and wing via the two sidestays, full symmetry of sidestays can hardly be achieved due to the difference in attachment points. In case the unreasonable design of structural parameters causes mutual restriction between the fore and aft sidestays, incomplete locking will be unavoidable. Thus, the motion coordination between the two sidestays appears particularly important.

4.1. Constraint Equations of DS Landing Gear. Figure 12 plots the schematic diagrams of a DS landing gear mechanism. Clearly, the mechanism comprises nine links, which has thirty-six independent geometric variables, and thirty-five independent constraint equations, as shown in the appendix. Compared to the SS mechanism, the number of constraint equations increases by sixteen. The superscripts f and a represent the relevant parameters of fore and aft sidestays, respectively, and the definitions of other parameters are consistent with those of the SS landing gear.

4.2. Singularity Analysis of DS Landing Gear. The retraction and extension processes of the DS landing gear can be simulated through numerically continuing the constraint equations, and the singular points and bifurcation curves of two sidestays can be derived, as shown in Figure 13. The ordinate θ_{oc} denotes the difference between angles of lock links, which is $\theta_{oc} = \theta_4 - \theta_5$ for the fore lock links and $\theta_{oc} = \theta_8 - \theta_9$ for the aft lock links.

Figure 13 shows the relationship between θ_{oc} and the retraction angle, where the grey and black lines represent the motion trajectories of the fore and aft lock links, respectively. The fore sidestay has three singular points ($S1^f$, $S2^f$, and $S3^f$). In contrast, the aft sidestay has only one singular point ($S1^a$). It can be seen intuitively that the fore lock links

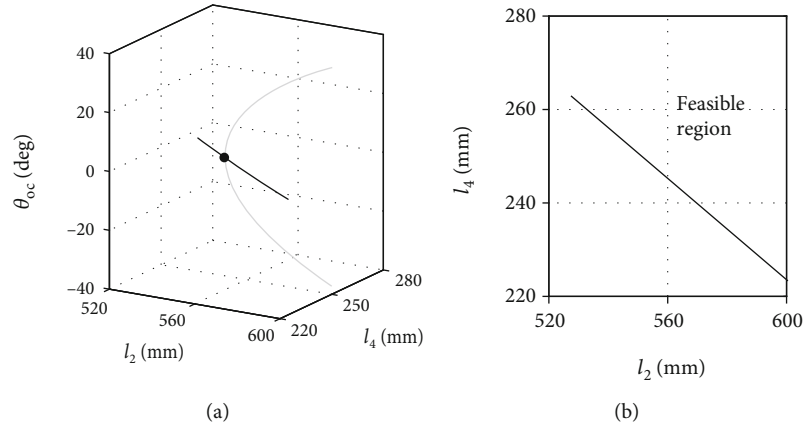

Figure 11: Bifurcation point SN variation under two-parameter continuation.

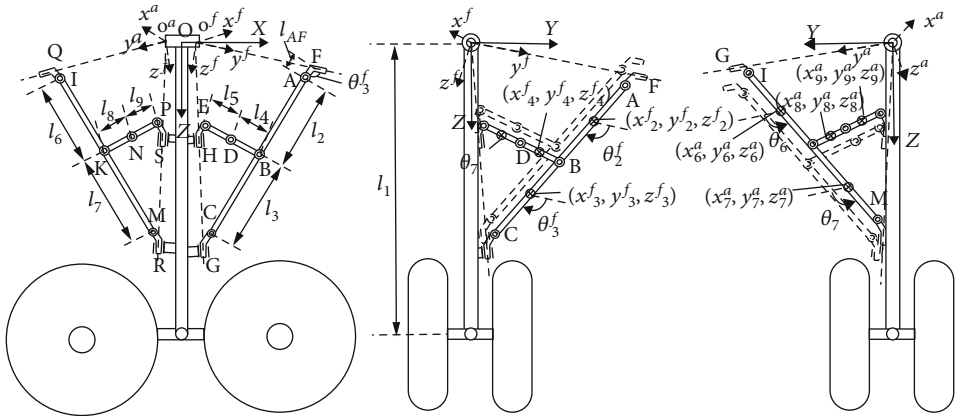

Figure 12: Schematic diagrams of the DS mechanism.

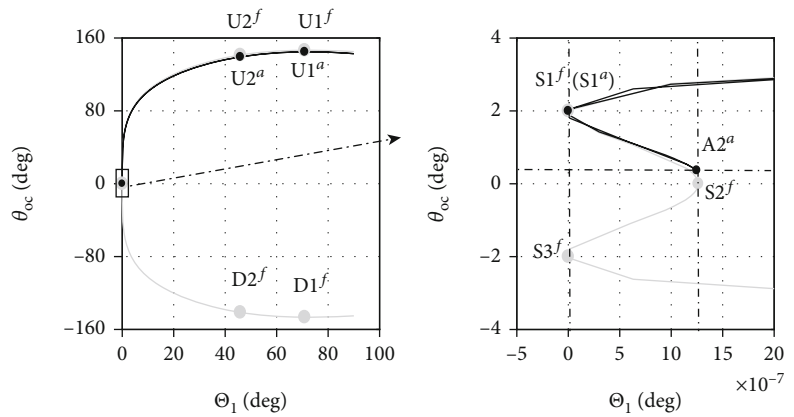

Figure 13: Bifurcation curves of DS landing gear.

can move to the area of $\theta_{oc} < 0$, while the aft lock links only move within the area of $\theta_{oc} > 0$. This indicates that the fore lock links can be locked, while the aft lock links cannot be locked. To better explain the motion of the studied landing gear, Figure 14 provides the kinematic sketches of mechanism that correspond to various points in Figure 13.

In Figure 14, the grey lines represent the fore sidestay, whereas the black lines represent the aft sidestay. It is not difficult to find that the sketches of fore and aft sidestays are similar in Figures 14(a)–14(c). When the fore sidestay reaches the singular point $S2^f$, the aft sidestay moves to point $A2^a$, as shown in Figure 14(d). At this time, the fore

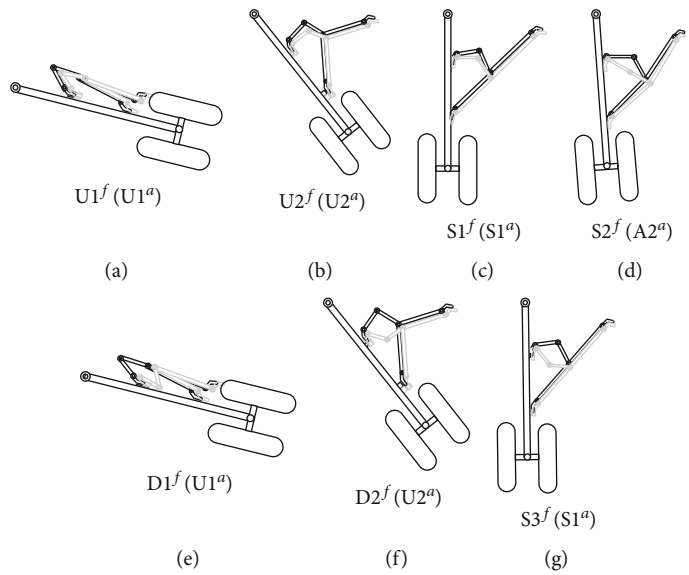

Figure 14: Sketches of DS mechanism motions: (a) U1^f(U1^a); (b) U2^f(U2^a); (c) S1^f(S1^a); (d) S1^f(A2^a); (e) D1^f(U1^a); (f) D2^f(U2^a); (g) S3^f(S1^a).

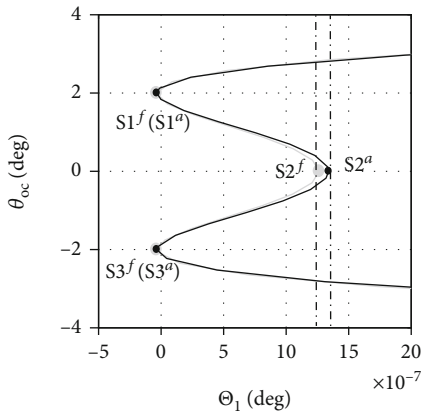

Figure 15: Independent computational results of the fore and aft sidestays.

lock links are collinear, while the aft lock links are still in the upper overcenter state. By the beneficial action of locking springs, the fore sidestay reaches the singular point S3^f, while the aft sidestay can only return to the singular point S1^a, as shown in Figure 14(g). As a result, only the fore sidestay is locked. Due to stop block, the landing gear does not move to the states shown in Figures 14(e) and 14(f) in reality.

To explain the reason that the aft sidestay cannot be fully locked, numerical continuation independently on the fore and aft sidestays is performed, as shown in Figure 15.

According to Figure 15, the motion trajectory of the aft sidestay also has three singular points when the two sidestays are computed separately, with S2^a appearing later than S2^f. When the landing gear reaches the point S1^f(S2^a), the main strut rotates to the farthest end, then begins to move backwards. At the time the fore sidestay reaches the point S2^f, the main strut has moved backwards to the farthest position (Figure 14(d)). To allow the aft sidestay to reach the S2^a point, the main strut needs to move continuously backwards to a position farther than S2^f. However, such motion is restricted by the fore sidestay, thereby creating a contradiction in motion coordination. Precisely, this contradiction of mutual restriction between the fore and aft sidestays is the fundamental reason why the DS landing gear is unable to be fully locked. To achieve complete locking, the retraction angle corresponding to the singular points S2^f and S2^a must be identical (i.e., $(\Theta_1)_{S2^f} = (\Theta_1)_{S2^a}$).

4.3. Effects of Link Length Parameters on the Synchronous Locking. In this section, the effects of link lengths on the singular points S2^f and S2^a are analyzed. It can be seen from Figure 15 that θ_{oc}^f and θ_{oc}^a are equal to zero at the points S2^f and S2^a. Hence, when considering the effects of points S2^f and S2^a, the parameters θ_{oc}^f and θ_{oc}^a can be used as the fixed parameters ($\theta_{oc}^f = \theta_{oc}^a = 0$), where Θ_1 is used as the state parameter, and the link lengths are used as the control parameters. Figure 16 plots the analytical results.

In Figure 16, the grey solid lines represent the influence of l_2 and l_4 on the singular point S2^f, while the black dashed lines represent the influence of l_6 and l_8 on the singular point S2^a. It is clear that the singular points exhibit generally consistent trends of variation with the link lengths. As described in the previous section, the synchronous locking can only be achieved when $(\Theta_1)_{S2^f} = (\Theta_1)_{S2^a}$. So once the value of Θ_1 is determined (e.g., $\Theta_1 = 0.1°$), the link lengths can be obtained intuitively, as shown by the dotted lines in Figure 16. The effects of variations in other link lengths can be analyzed in a similar way, which are thus not detailed herein.

Although changing the link lengths can yield $(\Theta_1)_{S2^f} = (\Theta_1)_{S2^a}$, it also changes the θ_{oc}^f and θ_{oc}^a in a deployed state.

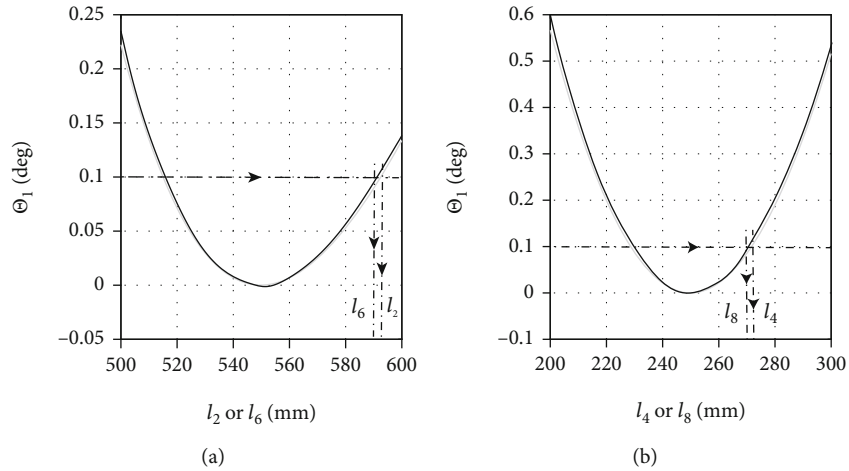

Figure 16: Curves describing the effects of link lengths on the second singular point.

Hence, a comprehensive consideration of the link lengths is needed based on multiple parameters.

4.4. Optimization of Synchronous Locking. In this section, an optimization is carried out to accomplish fully locking of the DS landing gear via the PSO, which is achieved by integrating ISIGHT with MATLAB for cosimulation analysis. Through optimization of link lengths, the fore and aft sidestays can be locked synchronously. PSO is a population-based optimization algorithm proposed by Kennedy and Eberhart [32] in 1995, who got inspiration from birds hunting for food. It initializes a system with a substantial number of random solutions and performs search for the optimal solution by updating generations. The PSO algorithm features very high probability of convergence to a global optimal solution, very fast computation, and strong global search ability. Existing research and applications indicate that PSO is a promising and effective optimization method [33–35]. Hence, the PSO algorithm is used for the optimization purpose in this paper.

As suggested in the foregoing analysis, θ_{oc}^{f} and θ_{oc}^{a} should not be excessively large when the landing gear is locked. Thus, the invariant overcenter angles of the lock links is used as one of the constraints, i.e., $(\theta_{oc}^{f})_{S3^f} = (\theta_{oc}^{a})_{S3^f} = 2^\circ$. Let $\Delta\Theta = |(\Theta_1)_{S2^f} - (\Theta_1)_{S2^a}|$; then, the synchronous locking of fore and aft sidestays necessitates $\Delta\Theta = 0$. The smaller the value of $\Delta\Theta$, the lesser the mutual restraint effect between the fore and aft sidestays. Accordingly, the optimization objective is set as min $\Delta\Theta$. The optimization variables are the lengths of various links. Due to the constraints, there are only four independent optimization variables, i.e., $l_i (i = 2, 4, 6, 8)$.

In Figure 17, the cosimulation-based optimization process is displayed, where the operators include the ISIGHT algorithm module and the MATLAB numerical continuation module. As a first step, the ISIGHT generates a set of initial parameters l_i based on the PSO algorithm and then passes the parameters to the MATLAB module. Afterwards, the MATLAB calculates the bifurcation points of the fore and aft sidestays based on the numerical continuation, as well as $\Delta\Theta$, $(\theta_{oc}^{f})_{S3^f}$, and $(\theta_{oc}^{a})_{S3^f}$, which are then transferred back to the ISIGHT. Finally, the ISIGHT identifies the optimal results that conform to the constraints.

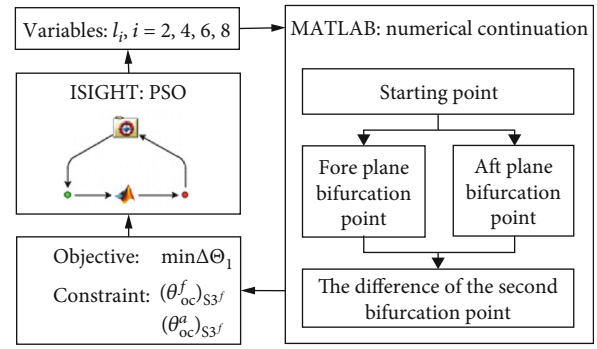

Figure 17: Computational flow of cosimulation-based optimization.

Since the change in link lengths leads to changed solutions of constraint equations, the starting point that satisfies the constraint equations is solved initially based on the PSO algorithm. To reduce the computational burden, the solution at $\Theta_1 = 5^\circ$ is chosen as the starting point. Afterwards, the singular points $S2^f$ and $S2^a$ are obtained through the parameter continuation analysis for reducing Θ_1, and the corresponding Θ_1 is identified. Finally, $\Delta\Theta$ is solved.

Based on the consideration of the mechanism motion interference, the optimization variables are set to $l_2 \in [450$ mm, 650 mm] and $l_6 \in [450$ mm, 650 mm], and the lock link lengths are set to $l_4 \in [200$ mm, 300 mm] and $l_8 \in [200$ mm, 300 mm]. The optimization results are shown in Tables 1 and 2 and Figure 18.

According to the optimization results in Figure 18, the points $S2^f$ and $S2^a$ are almost completely coincident, which allow simultaneous locking of the fore and aft sidestays, respectively, at $S2^f$ and $S2^a$. When the two sidestays are in a locked state, the angle between lock links remains constant at 2°.

Table 1: Synchronous locking optimization results.

	l_2	l_4	l_6	l_8	$\Delta\Theta$
Before	550 mm	250 mm	550 mm	250 mm	$7.72e-08^\circ$
Optimization	532.4655 mm	258.8501 mm	538.6727 mm	288.9462 mm	$2.24e-10^\circ$

Table 2: Synchronous locking optimization results (other parameters).

	l_3	l_5	l_7	l_9
Before	550 mm	260 mm	550 mm	260 mm
Optimization	567.5345 mm	261.2052 mm	561.3273 mm	227.5027 mm

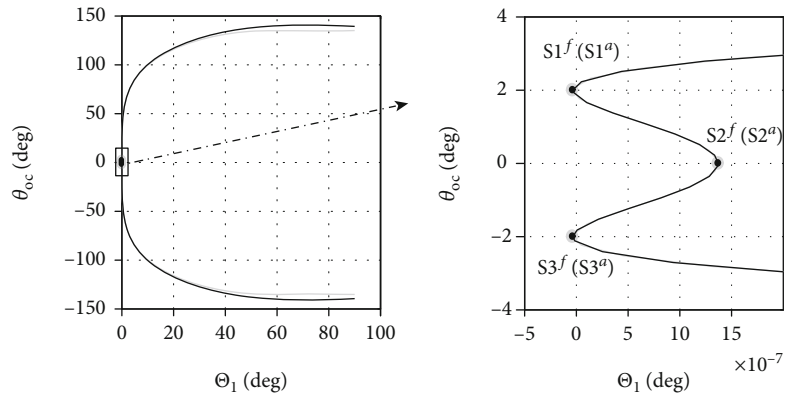

Figure 18: Singular points of dual-sidestay links after optimization.

5. Conclusion

A bifurcation theory-based method for analyzing the kinematics of sidestay landing gear locking mechanisms is proposed in this paper. Initially, the simple single-sidestay (SS) mechanism is analyzed, and then, the complex dual-sidestay (DS) mechanism is investigated based on SS. The main conclusions are as follows:

(1) Based on the bifurcation theory and singularity, the locked position of the SS landing gear is analyzed, clarifying that the lock links must be at the singular point of a lower overcenter angle, in order to achieve fully locking. Besides, the effect of link lengths on the locked position is analyzed, concluding that the link lengths should be within a feasible range

(2) For DS, the presence of an additional sidestay poses an adverse impact on the downward folding motion of lock links. The kinematic cause underlying the adverse impact is analyzed. Owing to the different positions of singular points, the movements of fore and aft sidestays seriously restrict each other, causing locking failure of the DS landing gear

(3) A kinematic optimization method for the synchronous locking of the DS landing gear is proposed. This study indicates that the full locking of the DS gear is achievable on condition that the overcenter angle of lock links is invariant.

Table 3: Parameters of the SS landing gear.

Parameters	Values
l_1 (mm)	1800
l_2 (mm)	550
l_3 (mm)	550
l_4 (mm)	250
l_5 (mm)	260
$(\alpha)_{\Theta_1=90}$ (deg)	115.3917
l_{AF} (mm)	98.6181
l_{CG} (mm)	60
l_{EH} (mm)	40
φ_{AF} (deg)	130.0157
$(\varphi_{CG})_{\Theta_1=0}$ (deg)	125
$(\varphi_{EH})_{\Theta_1=0}$ (deg)	105
$\mathbf{o_O}$ (mm)	(-69.2820, 39.1058, 8.4104)
$(\mathbf{e}_{21})_{\Theta_1=0}$ (mm)	(0.8660, -0.5000, 0)
$(\mathbf{e}_{22})_{\Theta_1=0}$ (mm)	(0.4888, 0.8467, 0.2103)
$(\mathbf{e}_{23})_{\Theta_1=0}$ (mm)	(-0.1051, -0.1821, 0.9776)
$(G)_{\Theta_1=0}$ (mm)	(105, 43.3013, 1000)
$(H)_{\Theta_1=0}$ (mm)	(92.5, 21.6506, 500)

Appendix

The motion constraint equations of the DS landing gear are as follows (Tables 3 and 4):

$$\begin{bmatrix} X_1 \\ Y_1\text{-}0.5l_1 \cdot \cos\Theta_1 \\ Z_1\text{-}0.5l_1 \cdot \sin\Theta_1 \\ x_2^f \\ y_2^f - 0.5l_2 \cdot \cos\theta_2^f - y_A^f \\ z_2^f - 0.5l_2 \cdot \sin\theta_2^f - z_A^f \\ x_3^f \\ y_3^f - 0.5l_3 \cdot \cos\theta_3^f\text{-}y_2^f - 0.5l_2 \cdot \cos\theta_2^f \\ z_3^f - 0.5l_3 \cdot \sin\theta_3^f\text{-}z_2^f - 0.5l_2 \cdot \sin\theta_2^f \\ x_4^f \\ y_4^f + 0.5l_4 \cdot \cos\theta_4^f\text{-}y_2^f - 0.5l_2 \cdot \cos\theta_2^f \\ z_4^f - 0.5l_4 \cdot \sin\theta_4^f\text{-}z_2^f - 0.5l_2 \cdot \sin\theta_2^f \\ x_5^f \\ y_5^f + 0.5l_5 \cdot \cos\theta_5^f\text{-}y_4^f + 0.5l_4 \cdot \cos\theta_4^f \\ z_5^f - 0.5l_5 \cdot \sin\theta_5^f\text{-}z_4^f + 0.5l_4 \cdot \sin\theta_4^f \\ y_5^f\text{-}0.5l_5 \cdot \cos\theta_5^f\text{-}y_E^f \\ z_5^f - 0.5l_5 \cdot \sin\theta_5^f\text{-}z_E^f \\ y_3^f + 0.5l_3 \cdot \cos\theta_3^f\text{-}y_C^f \\ z_3^f + 0.5l_3 \cdot \sin\theta_3^f\text{-}z_C^f \\ x_6^a \\ y_6^a - 0.5l_6 \cdot \cos\theta_6^a - y_I^a \\ z_6^a - 0.5l_6 \cdot \sin\theta_6^a - z_I^a \\ x_7^a \\ y_7^a - 0.5l_7 \cdot \cos\theta_7^a\text{-}y_6^a - 0.5l_6 \cdot \cos\theta_6^a \\ z_7^a - 0.5l_7 \cdot \sin\theta_7^a\text{-}z_6^a - 0.5l_6 \cdot \sin\theta_6^a \\ x_8^a \\ y_8^a + 0.5l_8 \cdot \cos\theta_8^a\text{-}y_6^a - 0.5l_6 \cdot \cos\theta_6^a \\ z_8^a - 0.5l_8 \cdot \sin\theta_8^a\text{-}z_6^a - 0.5l_6 \cdot \sin\theta_6^a \\ x_9^a \\ y_9^a + 0.5l_9 \cdot \cos\theta_9^a\text{-}y_8^a + 0.5l_8 \cdot \cos\theta_8^a \\ z_9^a - 0.5l_9 \cdot \sin\theta_9^a\text{-}z_8^a + 0.5l_8 \cdot \sin\theta_8^a \\ y_9^a\text{-}0.5l_9 \cdot \cos\theta_9^a\text{-}y_P^f \\ z_9^a - 0.5l_9 \cdot \sin\theta_9^a\text{-}z_P^f \end{bmatrix}$$

$$\begin{bmatrix} y_7^a + 0.5l_7 \cdot \cos\theta_7^a\text{-}y_M^f \\ z_7^a + 0.5l_7 \cdot \sin\theta_7^a\text{-}z_M^f \end{bmatrix} = 0, \quad (A.1)$$

Table 4: Parameters of the DS landing gear.

Parameters	Values
l_1 (mm)	1800
l_2 (mm)	550
l_3 (mm)	550
l_4 (mm)	250
l_5 (mm)	260
$(\alpha^f)_{\Theta_1=90}$ (deg)	115.3917
l_6 (mm)	550
l_7 (mm)	550
l_8 (mm)	250
l_9 (mm)	260
$(\alpha^a)_{\Theta_1=90}$ (deg)	111.4145
l_{AF} (mm)	98.6181
l_{CG} (mm)	60
l_{EH} (mm)	40
φ_{AF} (deg)	130.0157
$(\varphi_{CG})_{\Theta_1=0}$ (deg)	125
$(\varphi_{EH})_{\Theta_1=0}$ (deg)	105
l_{IQ} (mm)	98.6181
l_{MR} (mm)	60
l_{PS} (mm)	40
φ_{IQ} (deg)	130.0157
$(\varphi_{MR})_{\Theta_1=0}$ (deg)	125
$(\varphi_{PS})_{\Theta_1=0}$ (deg)	105
$\mathbf{o}_O^f$ (mm)	(-69.2820, 39.1058, 8.4104)
$\left(\mathbf{e}_{21}^f\right)_{\Theta_1=0}$ (mm)	(0.8660, -0.5000, 0)
$\left(\mathbf{e}_{22}^f\right)_{\Theta_1=0}$ (mm)	(0.4888, 0.8467, 0.2103)
$\left(\mathbf{e}_{23}^f\right)_{\Theta_1=0}$ (mm)	(-0.1051, -0.1821, 0.9776)
$(G)_{\Theta_1=0}$ (mm)	(105, 43.3013, 1000)
$(H)_{\Theta_1=0}$ (mm)	(92.5, 21.6506, 500)
$\mathbf{o}_O^a$ (mm)	(65.5322, -44.8604, 9.6280)
$(\mathbf{e}_{21}^a)_{\Theta_1=0}$ (mm)	(0.8192, -0.5736, 0)
$(\mathbf{e}_{22}^a)_{\Theta_1=0}$ (mm)	(-0.5608, 0.8008, 0.2103)
$(\mathbf{e}_{23}^a)_{\Theta_1=0}$ (mm)	(0.1206, -0.1722, 0.9776)
$(R)_{\Theta_1=0}$ (mm)	(-108.6788, 40.9576, 1000)
$(S)_{\Theta_1=0}$ (mm)	(-94.3394, 20.4788, 500)

where

$$\begin{bmatrix} y_A^f \\ z_A^f \\ y_C^f \\ z_C^f \\ y_E^f \\ z_E^f \\ y_I^a \\ z_I^a \\ y_M^a \\ z_M^a \\ y_P^a \\ z_P^a \end{bmatrix} = \begin{bmatrix} y_F^f + l_{\mathrm{AF}} \cdot \cos \varphi_{\mathrm{AF}} \\ l_{\mathrm{AF}} \cdot \sin \varphi_{\mathrm{AF}} \\ y_G^f - l_{\mathrm{CG}} \cdot \cos \varphi_{\mathrm{CG}} \\ z_G^f - l_{\mathrm{CG}} \cdot \sin \varphi_{\mathrm{CG}} \\ y_H^f - l_{\mathrm{EH}} \cdot \cos \varphi_{\mathrm{EH}} \\ z_H^f - l_{\mathrm{EH}} \cdot \sin \varphi_{\mathrm{EH}} \\ y_Q^a + l_{\mathrm{IQ}} \cdot \cos \varphi_{\mathrm{IQ}} \\ l_{\mathrm{IQ}} \cdot \sin \varphi_{\mathrm{IQ}} \\ y_M^a - l_{\mathrm{MR}} \cdot \cos \varphi_{\mathrm{MR}} \\ z_M^a - l_{\mathrm{MR}} \cdot \sin \varphi_{\mathrm{MR}} \\ y_P^a - l_{\mathrm{PS}} \cdot \cos \varphi_{\mathrm{PS}} \\ z_P^a - l_{\mathrm{PS}} \cdot \sin \varphi_{\mathrm{PS}} \end{bmatrix},$$

$$\begin{bmatrix} x_G^f \\ y_G^f \\ z_G^f \\ 1 \end{bmatrix} = T^f \cdot \begin{bmatrix} X_G \\ Y_G \\ Z_G \\ 1 \end{bmatrix},$$

$$\begin{bmatrix} x_H^f \\ y_H^f \\ z_H^f \\ 1 \end{bmatrix} = T^f \cdot \begin{bmatrix} X_H \\ Y_H \\ Z_H \\ 1 \end{bmatrix},$$

$$\begin{bmatrix} x_M^a \\ y_M^a \\ z_M^a \\ 1 \end{bmatrix} = T^a \cdot \begin{bmatrix} X_M \\ Y_M \\ Z_M \\ 1 \end{bmatrix},$$

$$\begin{bmatrix} x_P^a \\ y_P^a \\ z_P^a \\ 1 \end{bmatrix} = T^a \cdot \begin{bmatrix} X_P \\ Y_P \\ Z_P \\ 1 \end{bmatrix}. \quad (A.2)$$

Notations

$\mathbf{T}_0$, $\mathbf{T}_1$, $\mathbf{T}$: Transformation matrix of the global coordinate system to the local system
l_{AF}, l_{CG}, l_{EH}: The node lengths
l_i: The length of link i
$\mathbf{e}_1$, $\mathbf{e}_2$: The base vectors in the global and local coordinate systems
x_i, y_i, z_i: The local coordinate values at the center of gravity of the i-th link
X_i, Y_i, Z_i: The global coordinate values at the center of gravity position of the i-th link
l_{AF}, l_{CG}, l_{EH}: The node lengths
φ_{AF}, φ_{CG}, φ_{EH}: The angles of node axes with respect to the y-axis of local coordinates
Θ_i: The angle of the i-th link with respect to the Z-axis of global coordinates
θ_i: The angle of the i-th link with respect to the y-axis of local coordinates
α: The rotation angle of local coordinate system about the y-axis
θ_{d}: Overcenter angle of sidestay links
θ_{oc}: Overcenter angle of lock links
y_*, z_*: The local coordinate values at the positions of node $*$
Superscript f: The relevant parameters of fore sidestay
Superscript a: The relevant parameters of aft sidestay.

Data Availability

The geometry data used to support the findings of this study are included within the article.

Conflicts of Interest

The authors declare that they have no conflicts of interest.

Authors' Contributions

Kui Xu and Yin Yin contributed equally to this work.

Acknowledgments

This study was financially supported by the National Natural Science Foundation of China (51805249), the Natural Science Foundation of Jiangsu Province (BK20180436), the Fundamental Research Funds for the Central Universities (NF2018001), and the Priority Academic Program Development of Jiangsu Higher Education Institutes.

References

[1] E. N. Tinoco, O. P. Brodersen, S. Keye et al., "Summary data from the Sixth AIAA CFD Drag Prediction Workshop: CRM cases," *Journal of Aircraft*, vol. 55, no. 4, pp. 1352–1379, 2018.

[2] W. Niu, Y. Zhang, H. Chen, and M. Zhang, "Numerical study of a supercritical airfoil/wing with variable-camber technology," *Chinese Journal of Aeronautics*, vol. 33, no. 7, pp. 1850–1866, 2020.

[3] M. Kinsley-Jones, "Airbus Adopts Vickers VC10 landing gear concept for A350 XWB," https://www.flightglobal.com/news/articles/picturesairbus-adopts-vickers-vc10-landing-gear-concept-for-a350-xwb-214238/.

[4] SAFRAN-Group, "Messier–Dowty exhibits wide range of landing gear technology at Paris Air Show," https://www.safranmbd.com/actualites/actu-etcommuniques-de-presse/article/messier-dowty-exhibits-wide-range-494.

[5] J. Veaux, "New design procedures applied to landing gear development," *Journal of Aircraft*, vol. 25, no. 10, pp. 904–910, 1988.

[6] M. Hać and K. From, "Design of retraction mechanism of aircraft landing gear," *Mechanics and Mechanical Engineering*, vol. 12, no. 4, pp. 357–373, 2008.

[7] J. N. Daniels, "A method for landing gear modeling and simulation with experimental validation," *NAS*, vol. 1, no. 26, p. 201601, 1996.

[8] B. Krauskopf, H. M. Osinga, and J. Galán-Vioque, *Numerical Continuation Methods for Dynamical Systems (Springer)*, Springer, Dordrecht, 2007.

[9] E. Allgower and K. Georg, *Numerical Continuation Methods, an Introduction*, Springer Science & Business Media, 1991.

[10] Q. Xin and Z. Shi, "Bifurcation analysis and stability design for aircraft longitudinal motion with high angle of attack," *Chinese Journal of Aeronautics*, vol. 28, no. 1, pp. 250–259, 2015.

[11] J. A. C. Knowles, B. Krauskopf, and M. H. Lowenberg, "Numerical continuation applied to landing gear mechanism analysis," *Journal of Aircraft*, vol. 48, no. 4, pp. 1254–1262, 2011.

[12] S. Sharma, E. B. Coetzee, M. H. Lowenberg, S. A. Neild, and B. Krauskopf, "Numerical continuation and bifurcation analysis in aircraft design: an industrial perspective," *Philosophical Transactions of The Royal Society A Mathematical Physical and Engineering ences*, vol. 373, p. 2015, 2051.

[13] J. A. C. Knowles, B. Krauskopf, and M. Lowenberg, "Numerical continuation analysis of a three-dimensional aircraft main landing gear mechanism," *Nonlinear Dynamics*, vol. 71, no. 1-2, pp. 331–352, 2013.

[14] J. A. C. Knowles, M. H. Lowenberg, S. A. Neild, and B. Krauskopf, "A bifurcation study to guide the design of a landing gear with a combined uplock/downlock mechanism," *Proceedings of the Royal Society A: Mathematical, Physical and Engineering Sciences*, vol. 470, no. 2172, article 20140332, 2014.

[15] J. A. C. Knowles, B. Krauskopf, M. H. Lowenberg, S. A. Neild, and P. Thota, "Numerical continuation analysis of a dual-sidestay main landing gear mechanism," *Journal of Aircraft*, vol. 51, no. 1, pp. 129–143, 2014.

[16] J. A. C. Knowles, "Bifurcation study of a dynamic model of a landing-gear mechanism," *Journal of Aircraft*, vol. 53, no. 5, pp. 1468–1477, 2016.

[17] Y. Yin, S. A. Neild, J. Z. Jiang, J. A. C. Knowles, and H. Nie, "Optimization of a main landing gear locking mechanism using bifurcation analysis," *Journal of Aircraft*, vol. 54, no. 6, pp. 2126–2139, 2017.

[18] V. D. Tourassis and H. Marcelo, "Identification and analysis of robot manipulator singularities," *The International Journal of Robotics Research*, vol. 11, no. 3, pp. 248–259, 1992.

[19] J. P. Merlet, "Singular configurations of parallel manipulators and Grassmann geometry," *International Journal of Robotics Research*, vol. 8, no. 5, pp. 194–212, 1989.

[20] F. C. Park and J. W. Kim, "Singularity analysis of closed kinematic chains," *Journal of Mechanical Design*, vol. 121, no. 1, pp. 32–38, 1999.

[21] H. Zhou and K. L. Ting, "Path generation with singularity avoidance for five-bar slider-crank parallel manipulators," *Mechanism & Machine Theory*, vol. 40, no. 3, pp. 371–384, 2005.

[22] S. K. Ider, "Inverse dynamics of parallel manipulators in the presence of drive singularities," *Mechanism & Machine Theory*, vol. 40, no. 1, pp. 33–44, 2005.

[23] F. Xie, T. Li, and X. Liu, "Type synthesis of 4-DOF parallel kinematic mechanisms based on Grassmann line geometry and atlas method," *Chinese Journal of Mechanical Engineering*, vol. 26, no. 6, pp. 1073–1081, 2013.

[24] Q. Li and J. M. Herve, "Type synthesis of 3-DOF RPR-equivalent parallel mechanisms," *IEEE Transactions on Robotics*, vol. 30, no. 6, pp. 1333–1343, 2014.

[25] Y. Yin, N. Hong, F. Fei, W. Xiaohui, and N. Huajin, "Nonlinear assembly tolerance design for spatial mechanisms based on reliability methods," *Journal of Mechanical Design*, vol. 139, no. 3, 2017.

[26] Y. Yin, N. Hong, N. Huajin, and Z. Ming, "Reliability analysis of landing gear retraction system influenced by multifactors," *Journal of Aircraft*, vol. 53, no. 3, pp. 713–724, 2016.

[27] C. Gosselin and J. Angeles, "Singularity analysis of closed-loop kinematic chains," *IEEE Transactions on Robotics & Automation*, vol. 6, no. 3, pp. 281–290, 1990.

[28] C. Innocenti and V. Parenti-Castelli, "Closed-form direct position analysis of a 5–5 parallel mechanism," *Journal of Mechanical Design*, vol. 115, no. 3, pp. 515–521, 1993.

[29] J. I. Pritchard, "An overview of landing gear dynamics," *Journal of Aircraft*, vol. 38, no. 1, pp. 130–137, 1999.

[30] S. Kruse, M. Tiedemann, B. Zeumer, P. Reuss, and N. Hoffmann, "The influence of joints on friction induced vibration in brake squeal," *Journal of Sound & Vibration*, vol. 340, no. 4, pp. 239–252, 2015.

[31] N. S. Currey, *Aircraft Landing Gear Design: Principle and Practice*, AIAA, Washington D.C., 1988.

[32] J. Kennedy and R. Eberhart, "Particle swarm optimization," in *IEEE International Conference on Neural Networks-Conference Proceedings*, vol. 4, pp. 1942–1948, Perth, WA, Australia, 1995.

[33] J.-J. Shin and H. Bang, "UAV path planning under dynamic threats using an improved PSO algorithm," *International Journal of Aerospace Engineering*, vol. 2020, Article ID 8820284, 17 pages, 2020.

[34] C. Nami, K. Oka, M. Sato, A. Harada, and K. Muraoka, "Control-based robust CAS design for QTW-UAV via the multiple-model approach with particle swarm optimization," *International Journal of Aerospace Engineering*, vol. 2019, Article ID 9267059, 17 pages, 2019.

[35] Y. Liu, X. Zhang, X. Guan, and D. Delahaye, "Adaptive sensitivity decision based path planning algorithm for unmanned aerial vehicle with improved particle swarm optimization," *Aerospace Science and Technology*, vol. 58, pp. 92–102, 2016.